Article

Not peer-reviewed version

Microwave-Assisted Interzeolite Transformations

Stanislav Ferdov *

Posted Date: 3 December 2024

doi: 10.20944/preprints202412.0199.v1

Keywords: microwave synthesis; interzeolite transformation; hierarchical zeolites; pseudomorphism; zeolite engineering; top-down hierarchization

 doi:10.20944/preprints202412.0199.v1

Article

Microwave-Assisted Interzeolite Transformations

Stanislav Ferdov [1,2]

[1] Physics Centre of Minho and Porto Universities (CF-UM-UP), University of Minho, 4710-057 Braga, Portugal; sferdov@fisica.uminho.pt

[2] Laboratory of Physics for Materials and Emergent Technologies, LaPMET, University of Minho, 4710-057, Braga, Portugal

Abstract: Zeolite crystallization involves complex and overlapping kinetic and thermodynamic processes, posing significant challenges to achieving precise control, especially during short crystallization periods. Microwave-assisted heating has proven effective in acceleration of zeolite crystallization from gel growth media, but its application to synthesis by interzeolite transformations is unknown. Herein, microwave-assisted heating is introduced as a method for interzeolite transformation demonstrating transformation of **FAU** zeolite to **CAN**, **ANA**, **EDI**, and **MER** zeolites. The microwave approach ensures interzeolite transformations within 5-10 min, which is tenths of times faster than transformations by conventional heating. This work also shows how at identical synthesis conditions the concentration of KOH directs the structure of the run product. Furthermore, the temperature control of the interzeolite transformation allows the production of pseudomorphic hierarchical particles of FAU zeolite in just 10 min without using any templating additives.

Keywords: microwave synthesis; interzeolite transformation; hierarchical zeolites; pseudomorphism; zeolite engineering; top-down hierarchization

1. Introduction

Zeolites are hydrated aluminosilicates whose active synthesis began in the 1950s, driven by their commercialization in separation and purification processes [1]. Initially, the zeolite production has been based on the hydrothermal conversion of aluminosilicate gels. Over time, this method proved effective not only for zeolites but also for a variety of chemically different zeolite-like materials [2,3] and for many years, gel-based synthesis remained the dominant method. However, in the pursuit of faster, more sustainable, and better-controlled synthesis, an alternative technique - interzeolite transformation (IZT) has reemerged, building on the early works of Barrer [4]. The IZT method involves the hydrothermal [5] or room temperature [6] transformation of a pre-existing ("parent") zeolite into a structurally different "daughter" zeolite. This approach has gained significant attention due to its simplicity and potential advantages, including faster crystallization, the ability to produce frameworks with a high Si/Al ratio and advanced pore chemistry, the creation of hierarchical structures, and the ability to achieve low synthesis temperatures that are often difficult to reach using conventional gel-based zeolite synthesis [6–11]. It is important to note that IZT should not be confused with the polymorphic transformations that occur during zeolite crystallization from a gel medium, where no parent phase is involved. Among the parent phases, FAU-type zeolite is one of the most studied due to its wide availability, cost-effective synthesis, and low-density framework, which allows transformations into a range of lower-density zeolites [12]. One such transformation is the conversion of **FAU** to **MER**-type zeolite, reported by Kirschhock and colleagues in 2013 [13]. They used an Rb- and Na-containing hydroxide solution and **FAU** zeolite with a Si/Al ratio of 2.6, obtaining **MER** zeolite after 96 hours at 95 °C. Similarly, Chengyu et al. later reported the synthesis of **MER** zeolite by transforming NaY and HY-**FAU** (Si/Al = 2.4-2.6) zeolites in a K-containing solution at 100–150 °C for 96 hours [14]. **MER** zeolite was also obtained under dry conditions by the mechanochemical treatment of **FAU** zeolite (Si/Al = 2.4) with KOH at 110 °C for 120 min [15]. Additionally, the conversion of clinoptilolite-rich natural zeolite to **MER** has been reported [16].

 doi:10.20944/preprints202412.0199.v1

EDI zeolite, another potassium-containing zeolite, was recently synthesized by IZT of **FAU** in concentrated KOH solutions, either at room temperature for 11–35 days or at 60 °C for 6–27 hours [6]. The IZT resulting in **ANA**-type structures was reported in 1999 by Chiyoda and Davis, who transformed NaY (Si/Al = 2.0–3.0) into **ANA** zeolite using sodium-containing solutions [17]. In 2010, Wang et al. synthesized **ANA** zeolite crystals with a regular icositetrahedron morphology by transforming ultrastable zeolite Y (Si/Al = 6.7) in NaOH solution at 100 °C for 42–288 hours [18]. In 2013, Kirschhock and colleagues also synthesized synthetic pollucite (**Cs-ANA**) by IZT of **FAU** zeolite (Si/Al = 2.6) in CsOH solution at 95 °C for 48 hours [13] More recently, **ANA** zeolite was synthesized through mechanochemically-assisted transformation of commercial **FAU** (Si/Al = 2.4) using CsOH or NaOH at 110°C for 120 min [15]. **CAN** zeolite was also synthesized under similar conditions using KOH [15]. Notably, the mechanochemically-assisted transformations of **FAU** are faster than the conventional synthesis of **MER** and **ANA**, which typically take 6 hours [19] and 5–10 hours [20], respectively.

While various types of radiation, such as UV light [21,22], gamma rays [23], and microwaves [24], have been used to control and accelerate zeolite crystallization from gel media, similar methods have not yet been applied to IZT-based synthesis. Microwave-assisted synthesis has been effective in accelerating conventional zeolite synthesis, including **MER** (180 °C for 12 min) [25], **ANA** (120 °C for 5h) [26], and **Li-EDI** (90 °C for 60 min) [27], among many others. However, this approach remains unexplored for IZT-based zeolite synthesis.

This work aims to introduce the first examples of microwave-assisted interzeolite transformation and show how this method can significantly accelerate crystallization. It also explores its potential for controlling zeolite crystal morphology, particle size, and crystal structure.

2. Results and Discussion

Four single-phase zeolite-type structures (**EDI**, **MER**, **CAN**, and **ANA**) were obtained by the transformation of **FAU** zeolite through hydrothermal treatment under microwave radiation. **Table 1** compares the fastest reported IZTs leading to **EDI**, **MER**, **CAN**, and **ANA** zeolites and the same phases obtained in this work. The microwave-assisted synthesis at higher temperatures assures at least 20 times faster crystallization than the mechanochemically-assisted and at least 70 times faster than the conventional heating approach. Additionally, a non-zeolitic aluminosilicate with a **Kalsilite** ($KAlSiO_4$) [28] structure was obtained.

Table 1. Comparison of the time and temperature of interzeolite and related transformations starting from **FAU** zeolite.

IZT	Heating	Time	Temp (°C)	Ref.
FAU→MER	Conventional	4 d	95	[13]
FAU→Cs-ANA	Conventional	2 d	95	[13]
FAU→EDI	Conventional	6 h	60	[6]
FAU→Na-ANA	Conventional & MC	2 h	110	[15]
FAU→Cs-ANA	Conventional & MC	2 h	110	[15]
FAU→MER	Conventional & MC	2 h	110	[15]
FAU→ANA	Conventional & MC	2 h	110	[15]
FAU→CAN	Conventional & MC	2 h	110	[15]
FAU→Kalsilite*	Microwave	10 min	160	This work
FAU→MER	Microwave	5 min	150-170	This work
FAU→Cs-ANA	Microwave	10 min	160	This work
FAU→EDI	Microwave	5 min	160	This work
FAU→CAN	Microwave	10 min	160	This work

MC – mechanochemical; * K-feldspar [29].

EDI-type zeolite was obtained for 5 min (160 °C), 10 min (160 °C), 1h (80 °C), 6h (60 and 80 °C), and 22h (60 °C) at two different KOH/FAU and H_2O/KOH ratios **(Figure 1a)**. In the system where

 doi:10.20944/preprints202412.0199.v1

KOH/**FAU**= 8.94, H_2O/KOH = 0.87 at 80 °C and within 22h occurs the transformation **FAU-EDI-Kalsilite (Figure 1b)** that follows a path from a more porous to less porous structure (**FAU** 12MR > **EDI** 8MR > **Kalsilite** 6MR) **(Figure 1c)**. The framework density (FD) change also follows the general rule of transformation from less to more dense structure (FD_{Si}: **FAU** 13.3 T/1000 > **EDI** 16.3 T/1000 > **Kalsilite** 19.9 T/1000 Å^3) indicating that the thermodynamically more stable phase has more framework atoms per unit volume. From a symmetry point of view, **FAU** (cubic) -**EDI** (tetragonal) -**Kalsilite** (hexagonal) transformations represent a sequence of change from higher to lower symmetry. At 60 °C, **FAU-EDI** transformation takes 6 h and after its formation **EDI** structure remains stable up to 22 hours, with the main difference being the relatively higher peak intensity when the synthesis time is longer **(Figure 1d)**. At the same (6h) or shorter (10 min) time for synthesis but at higher temperatures (120 °C and 160 °C) the run product of **FAU** transformation is **Kalsilite (Figure 1e)**. These results highlight the importance of temperature for control of **FAU-EDI** zeolite. The agitation speed during crystallization was found also to influence the IZT. While at 10 rpm and 60 °C **FAU** transforms to **EDI**, when the agitation speed is increased to 600 rpm the run product is an amorphous phase **(Figure 1f)**. In the studied systems it was observed that at low temperatures (60-80 °C), a low homogenization speed (10 rpm) favors the formation of a single daughter phase while a high homogenization speed (1200 rpm) at higher temperatures (150-170 °C) favors the formation of a single phase, which determined the choices of homogenization speed listed in **Table 2**.

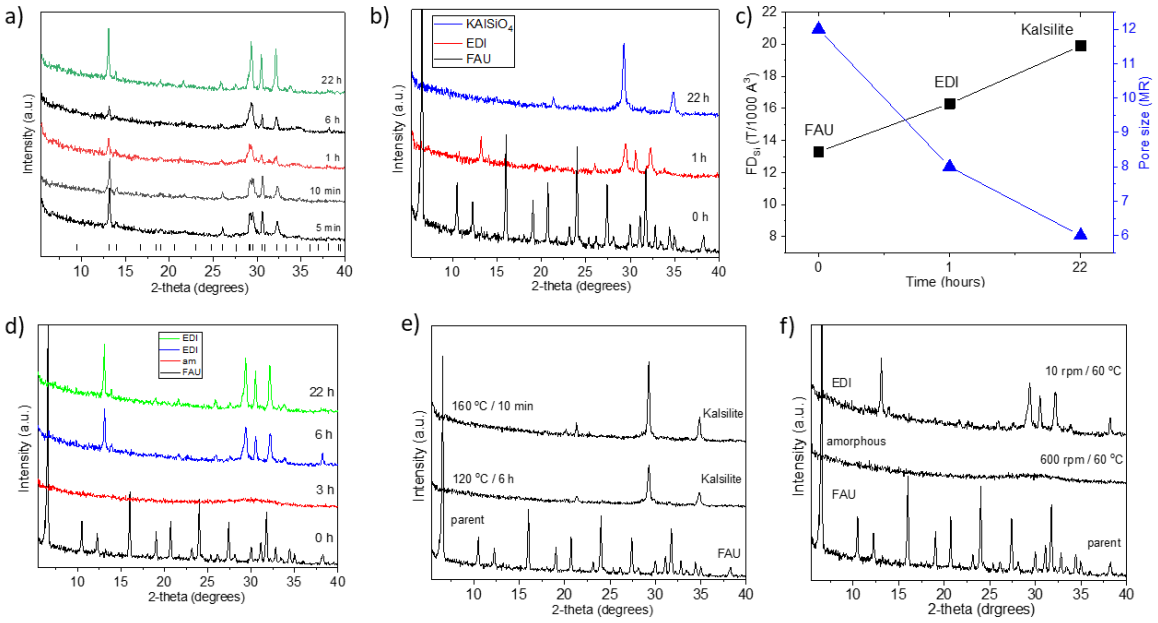

Figure 1. (a) Powder XRD patterns of **EDI** zeolite obtained by IZT of **FAU** zeolite for 5 min (160 °C), 10 min (160 °C) [KOH/**FAU**= 2, H_2O/KOH = 2], 1 h (80 °C), 6 h (60 °C) and 22 h (60 °C) [KOH/**FAU**= 8.94, H_2O/KOH = 0.87] (the vertical lines show the calculated peak positions). **(b)** Powder XRD patterns showing time-dependent **FAU-EDI-Kalsilite** transformation at 80 °C (KOH/**FAU** = 8.94 and H_2O/KOH = 0.87). **(c)** A diagram showing the changes of framework density and pore size during **FAU-EDI-Kalsilite** transformation. **(d)** Powder XRD patterns showing time-dependent **FAU-EDI** transformation at 60 °C. **(e)** Powder XRD patterns showing **EDI-Kalsilite** transformation at different temperatures [KOH/**FAU**= 8.94, H_2O/KOH = 0.87]. **(f)** Powder XRD patterns show the influence of homogenization speed on the **EDI-FAU** transformation at 60 °C [KOH/**FAU**= 8.94, H_2O/KOH = 0.87].

Table 2. Synthesis condition and phases obtained by IZT.

Parent Phase	Temperature (°C)	rpm	KOH/FAU	H_2O/KOH	Time	Daughter Phase/s
FAU	60	10	8.94	0.87	3 h	**am**
FAU	60	600	8.94	0.87	6 h	**am**

 doi:10.20944/preprints202412.0199.v1

FAU	60	10	8.94	0.87	6 h	**EDI**
FAU	60	10	8.94	0.87	22 h	**EDI**
FAU	80	10	8.94	0.87	6 h	**EDI**
FAU	80	10	8.94	0.87	22 h	**$KAlSiO_4$**
FAU	80	600	8.94	0.87	10 min	**am**
FAU	80	10	8.94	0.87	3 h	**$KAlSiO_4$**
FAU	80	10	0.4	19.5	22 h	**FAU, CHA**
FAU	80	10	8.94	0.87	1 h	**EDI**
FAU	80*		8.94	0.87	1 h	**am**
FAU	100	10	2	4.5	10 min	**FAU**
FAU	100	20	0.62	12.6	11 h	**CHA, GME, MER, NAT**
FAU	100	20	0.62	12.6	15 h	**CHA, GIS, MER**
FAU	100	20	0.60	13	22 h	**CHA, GME, MER**
FAU	120	10	8.94	0.87	6 h	**$KAlSiO_4$**
FAU	120	10	2	4.5	10 min	**FAU**
FAU	130	1200	2	4.5	10 min	**FAU**
FAU	140	1200	2	4.5	10 min	**FAU**
FAU	150	10	2	4.5	10 min	**CHA, GME, GIS**
FAU	150	1200	2	4.5	5 min	**MER**
FAU	160	10	1	4.5	5 min	**CHA, GME, MER**
FAU	160	10	1	9	10 min	**GME, GIS, AMI, CHA**
FAU	160	10	2	4.5	10 min	**CHA, GME**
FAU	160	10	2[a]	4.5	10 min	**CAN**
FAU	160	10	8.94	0.87	10 min	**$KAlSiO_4$**
FAU	160	1200	0.56	16.1	10 min	**ANA, GIS**
FAU	160	1200	0.6	15	1 h	**MER**
FAU	160	1200	0.7	4.5	10 min	**MER**
FAU	160	1200	1	4.5	10 min	**MER**
FAU	160	1200	1.42[b]	4.9	10 min	**Cs-ANA**
FAU	160	1200	2	1	10 min	**$KAlSiO_4$**
FAU	160	1200	2	2	5 min	**EDI**
FAU	160	1200	2	2	10 min	**EDI**
FAU	160	1200	2	3	10 min	**EDI, GIS**
FAU	160	1200	2	4	10 min	**EDI, GIS, PHI**
FAU	160	1200	2	4.5	1 min	**FAU**
FAU	160	1200	2	4.5	5 min	**CHA, GME**
FAU	160	1200	2	4.5	10 min	**CHA, MER**
FAU	160	1200	2	5	10 min	**GIS, PHI, MER**
FAU	170	10	2	4.5	10 min	**PHI, MER, NAT, $Na_2Si_4O_9$**
FAU	170	20	2.7[b]	2.59	1 h	**ANA**
FAU	170	1200	2	4.5	10 min	**MER**

[a] NaOH, [b] CsOH, am - amorphous.

 doi:10.20944/preprints202412.0199.v1

Figure 2a shows the time-temperature dependence of transformations of **FAU** zeolite in a system where KOH/**FAU** = 8.94 and H_2O/KOH = 0.87. In general, the higher temperature accelerates the **FAU**-**EDI** transformation and at 80 °C it occurs just in 1h while at 60 °C the same process takes 6h. At more prolongated times for crystallization (22h) the low temperature (60 °C) results in **EDI** zeolite while for the same time of crystallization at 80 °C is formed **Kalsilite**. At much high temperatures (120 °C, 160 °C) the transformation **FAU**-**Kalsilite** occurs rapidly (10-60 min), and no EDI zeolite was captured. **Figure 2b** shows a field of crystallization with compositions that yield a single phase **EDI**, **MER** zeolite, and **Kalsilite** at 160 °C for 10 min of synthesis. The powder XRD patterns of phases obtained after synthesis at different H_2O/KOH ratios are shown in **Figure 2c.** It appears that at short times for crystallization and higher temperature, the capturing of **EDI** zeolite requires lower KOH/**FAU** (2) and higher H_2O/KOH (2) ratios compared to those at the low-temperature conditions in **Figure 2a.** The crystallization of phase pure **MER** zeolite is localized at KOH/**FAU** = 0.7-2.0 and H_2O/KOH = 4.5. Compared to **EDI** zeolite it is clear that the synthesis of **MER** zeolite requires a higher H_2O/KOH ratio. Independent of the KOH/**FAU** ratio (2-9) the high temperature promotes the crystallization of **Kalsilite**. **Figure 2b** demonstrates how adjusting the H_2O/KOH ratio, while maintaining a constant KOH/FAU ratio of 2, influences the crystallization process. As the amount of KOH in the synthesis mixture decreases, the sequence of zeolite formation shifts. In particular, the sequence of formation of **Kalsilite**, **EDI** and **MER** follow the progressive reduction of KOH concentration, with a low amount of KOH favoring the crystallization of **MER**, while a high one favors the transformation into **EDI** zeolite and **Kalsilite**, respectively. When the H_2O/KOH ratio deviates from the optimal value needed for the crystallization of a single-phase zeolite, secondary phases like **GIS** and **PHI** (**HAR**) begin to form. This is shown in **Figure 2c,d,** where varying the H_2O/KOH ratio from the optimal value results in secondary phases. The appearance of these phases reveals the importance of alkalinity for selection of the daughter phase.

From thermodynamic perspective, the alkalinity of the solution directly impacts the Gibbs free energy (ΔG) of dissolution and hence the availability of silica and alumina species for zeolite formation. Therefore, the fine balance of solubility of silica and alumina controlled by the KOH concentration determines the availability of these species for formation of certain zeolite structure. The relationship between the H_2O/KOH ratio in the growth solution and the K/(Al+Si) ratio in the parent phase shows that higher KOH concentrations reduce the free energy of formation for K-rich phases, making their formation thermodynamically favorable **(Figure 2e)**. Considering these results one can suggest that the alkalinity not only lowers the nucleation barrier but also influences which crystalline phase forms by affecting the supersaturation levels for different phases (different polymorphs or phases have distinct solubility products and free energy profiles), interfacial energy surfaces (high alkalinity can reduce the surface energies for specific phase, thus lowering the nucleation barrier compared to other phases) and finally promote kinetically favorable phases due to rapid nucleation under high supersaturation.

Preprints.org (www.preprints.org) | NOT PEER-REVIEWED | Posted: 3 December 2024 doi:10.20944/preprints202412.0199.v1

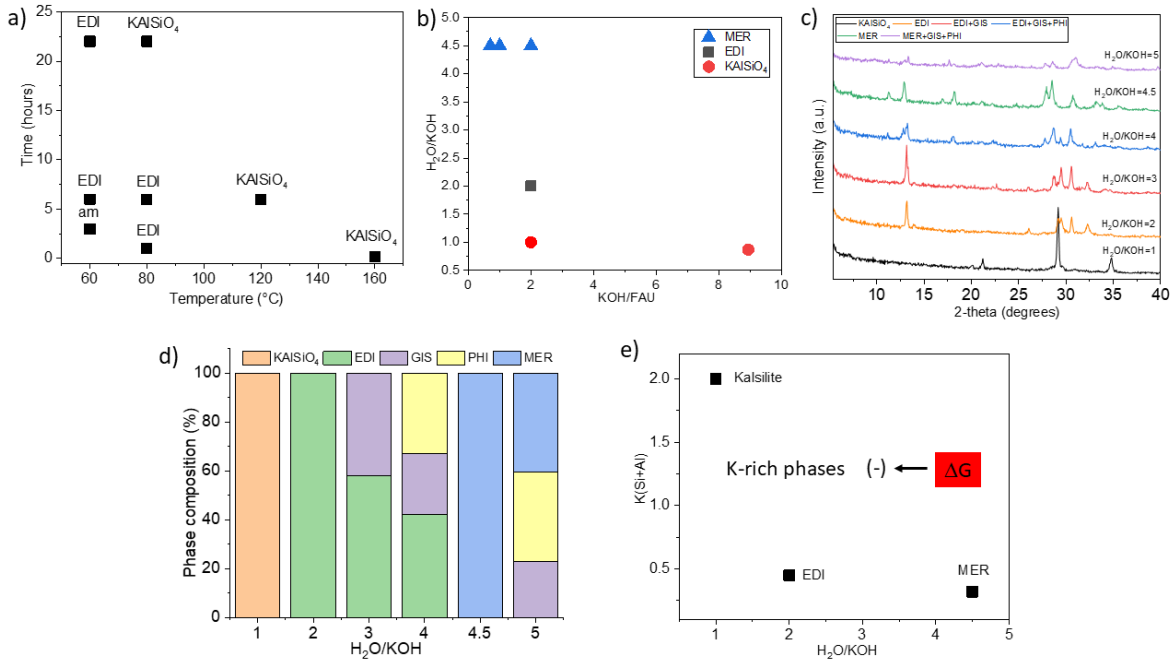

Figure 2. (a) Time/temperature relationships during IZT of **FAU** at KOH/**FAU** = 8.94 and H_2O/KOH = 0.87. **(b)** Selected compositions from the field of crystallization yielding phase pure materials at 160 °C for 10 min. **(c)** Powder XRD patterns showing the transformation of **FAU** zeolite at 160 °C for 10 min after changing the H_2O/KOH ratio at fixed KOH/**FAU** = 2. **(d)** Composition of the run product obtained after transformation of **FAU** zeolite at 160 °C for 10 min at different H_2O/KOH ratio. **(e)** Relationship between the H_2O/KOH ratio in the growth solution and the K/(Al+Si) ratio in the parent phase. Rising alkalinity affects both the nucleation barrier and phase selection.

Compared to the same IZT using conventional heating [6], the transformation of **FAU** to **EDI** via microwaves shows different results. At low temperature (60 °C), the transformation time (6 hours) is similar for both microwave and conventional heating methods. However, when the temperature is increased to 80 °C, microwave heating drastically reduces the crystallization time to just 1 hour, whereas with conventional heating, the product remains amorphous after the same duration (**Figure S2**). These results suggest that above a certain temperature, microwaves play a crucial role in accelerating crystallization.

Figure 3a shows the powder XRD patterns of samples obtained from kinetic studies conducted at KOH/**FAU** = 2.0 and H_2O/KOH = 4.5 at 160 °C. The changes in the diffractograms reveal that the IZTs are highly sensitive to the crystallization time. After 1 min of synthesis, the parent FAU structure is mostly preserved, but a peak shift towards smaller 2-theta angles is observed. The refinement of the unit cell shows a lattice parameter a = 24.93 Å, which corresponds to Si/Al = 1.3 and indicates a transformation of the parent zeolite Y into zeolite X. After 5 min of synthesis, the FAU structure transforms into a mixture of **MER**, **CHA** and **GME** zeolites. After 10 min of heating crystallize phase pure **MER** zeolite, which, after 60 min, transforms into a mixture of **MER** and **NAT** zeolites (**Figure 3b**). These results demonstrate that the IZTs are effectively controlled by the crystallization time.

MER zeolite was also obtained after 5 min at 150 °C and 1h at 160°C (**Figure S1**). The synthesis of **MER** zeolite is temperature-sensitive: at 150 °C, 160°C, or 170 °C, **MER** crystallizes in 10 min, but when the temperature is reduced to 140 °C, the parent **FAU** zeolite is preserved but with larger unit cell.

Figure 3c shows powder XRD patterns of the phases obtained after 10 min of synthesis at different temperatures in the system KOH/**FAU** = 2 and H_2O/KOH = 4.5. At 130 °C and 140 °C, the parent **FAU** structure is maintained, but there is a shift of XRD reflections (in the 20-35° 2θ range) towards smaller angles. The refined powder XRD pattern revealed a **FAU** unit cell (a = 24.91 Å) that corresponds to a Si/Al ratio of 1.3. This value is slightly lower than the value determined by EDS

 doi:10.20944/preprints202412.0199.v1

analysis (1.7), which indicates the presence of an amorphous silica. The lowest temperature at which **MER** zeolite crystallizes is 150 °C. At 160 °C, **MER** zeolite also forms but with lower crystallinity compared to the phase obtained at 170 °C.

Figure 3d shows the powder XRD patterns for the transformation of **FAU** to **ANA** and **FAU** to **CAN** zeolites. The **FAU**-**ANA** IZT was achieved at CsOH/**FAU** = 2.7 and H_2O/CsOH = 2.59 (at 170 °C for 1 hour), resulting in **Cs-ANA** with a Si/Al ratio of 3.3. A similar **FAU**-**ANA** transformation occurred at CsOH/**FAU** = 1.42 (at 160 °C for 10 min) with H_2O/CsOH = 4.9, producing **Cs-ANA** with a Si/Al ratio of 2.6. The shorter synthesis time and lower temperature led to more intense XRD reflections, indicating improved crystallinity. These results demonstrate that both the framework composition and crystallinity can be effectively controlled by adjusting the synthesis conditions. **CAN** zeolite was synthesized at NaOH/**FAU** = 2 and NaOH/CsOH = 4.5 at 160 °C for 10 min, resulting in framework with a Si/Al ratio of 1.2.

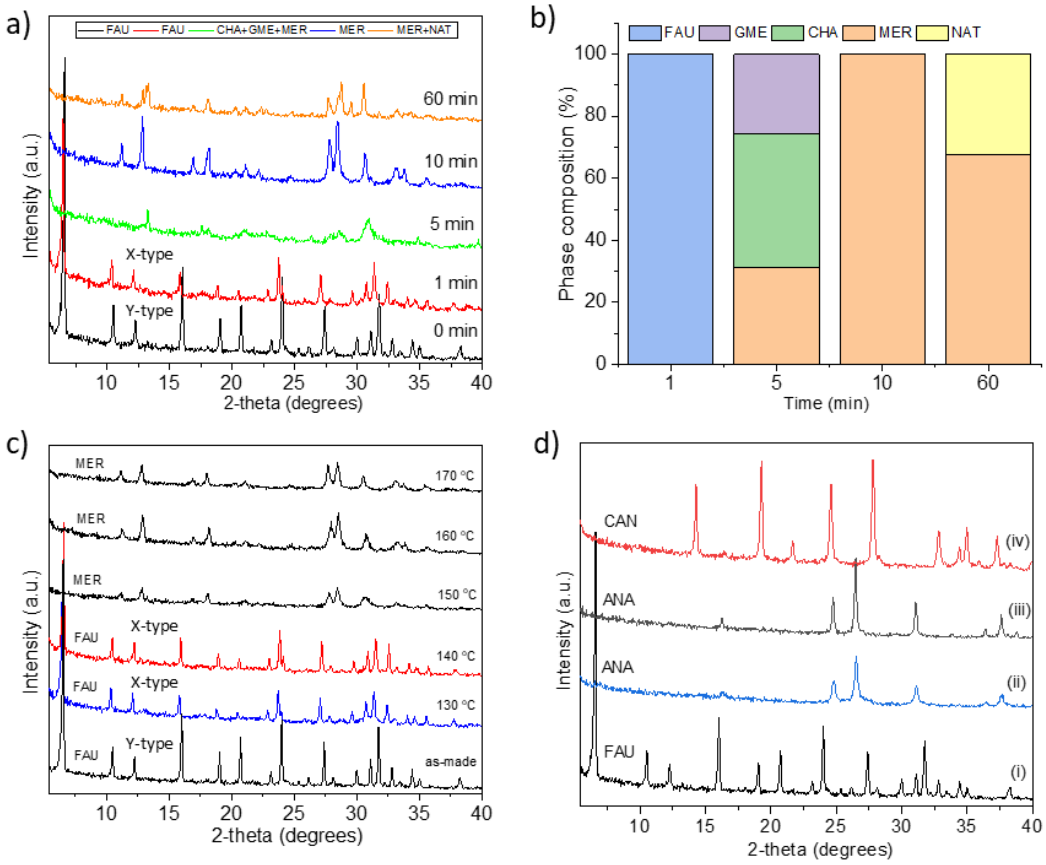

Figure 3. (a) Powder XRD patterns showing the transformation of **FAU** zeolite at different times at 160 °C KOH/**FAU** = 2 and H_2O/KOH = 4.5. **(b)** Phase composition of the run product after different times for synthesis. **(c)** Powder XRD patterns of zeolites obtained by IZT of **FAU** at different temperature in the system KOH/**FAU** = 2 and H_2O/KOH = 4.5. **(d)** Powder XRD patterns of transformation of (i) **FAU** to **ANA** zeolite at CsOH/**FAU** = 2.7 and H_2O/CsOH = 2.59 (170 °C for 1h). (iii) **ANA** zeolite at CsOH/**FAU** = 1.42 (160 °C for 10 min) and H_2O/CsOH = 4.9. (iv) **CAN** zeolite obtained at NaOH/**FAU** = 2 and NaOH/CsOH = 4.5 at 160 °C for 10 min.

Figure 4a shows an SEM image of the parent **FAU** zeolite transformed into hierarchical **FAU** **(Figures 4a-c)** and MER zeolites **(Figures 4d-f)**. The **FAU** samples obtained after synthesis at 130 °C **(Figure 4b)** and 140 °C **(Figure 4c)** (with KOH/**FAU** = 2 and H_2O/KOH = 4.5) exhibit hierarchical structures formed by the dissolution of the parent **FAU** phase. This dissolution occurs in such a way that the initial shape of the **FAU** particles is retained, but numerous nanofins are carved into the psrent particles. Compared to previous examples of post-synthetic treatment of **FAU** zeolites that

 doi:10.20944/preprints202412.0199.v1

result in hierarchal structures [10,30,31], the microwave-assisted approach show potential for more simple (organic-free) and faster crystal hierarchization. By keeping the initial batch composition, the same but increasing the synthesis temperature to 150 °C **(Figure 4d)**, 160 °C **(Figure 4e)**, or 170 °C **(Figure 4f)**, the **FAU** zeolite transforms into **MER** zeolite with Si/Al ratio = 1.6–1.7. At the higher synthesis temperature (170 °C), the **MER** zeolite crystals are better faceted and more abundant compared to those obtained at the lower temperatures.

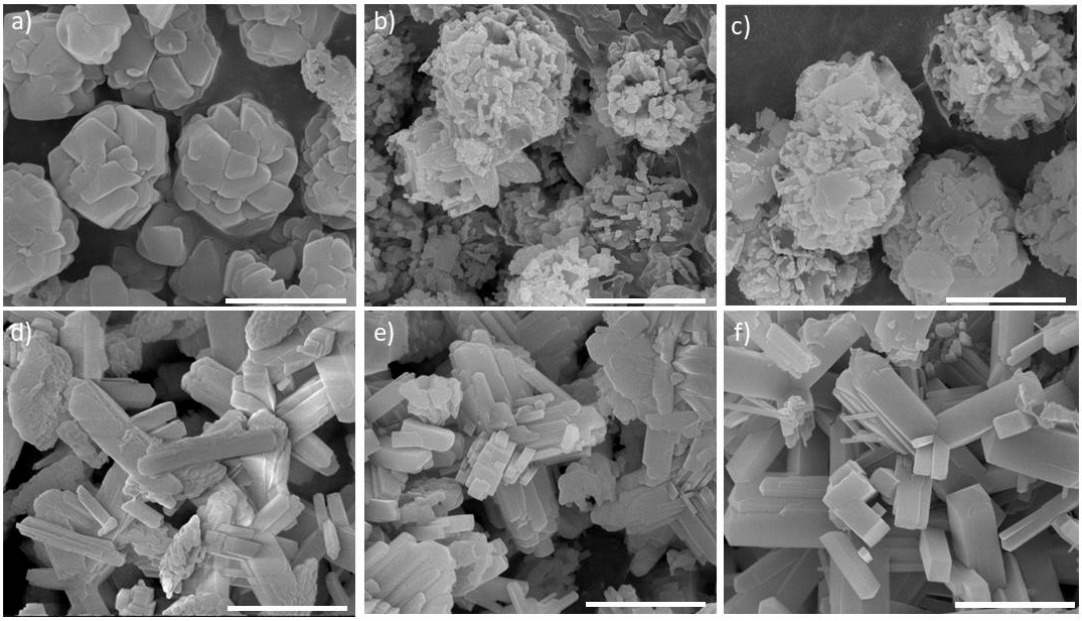

Figure 4. SEM images of **(a)** the parent and the daughter hierarchical **FAU** zeolites obtained at **(b)** 130 °C and **(c)** 140 °C. Daughter **MER** zeolites obtained at **(d)** 150 °C, and **(e)** 160 °C and **(f)** 170 °C. Bar = 2 μm.

Figure 5 shows a schematic model of the pathways of **FAU** transformation where the parent **FAU** can be selectively transformed to hierarchal **FAU** with a lower Si/Al ratio or to a **MER** zeolite. The transformation is controlled by simple temperature adjustment that has previously been shown to have a significant effect on the crystallization route [32].

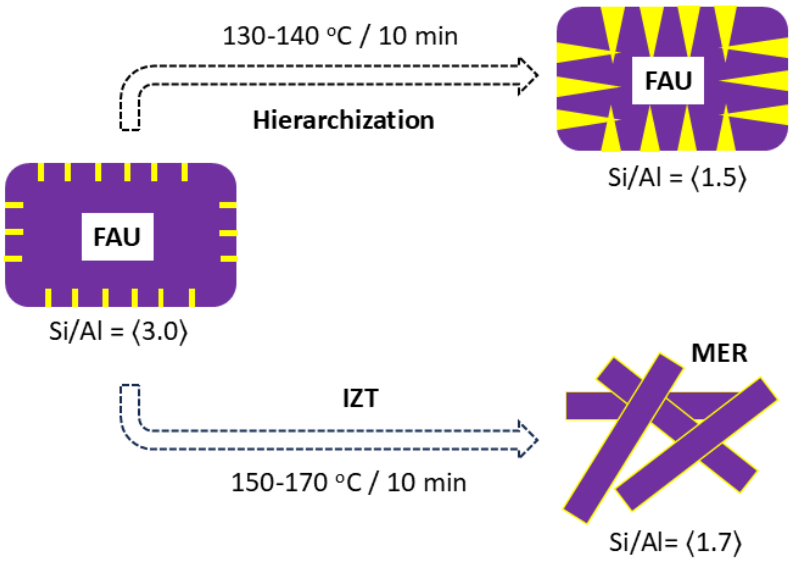

 doi:10.20944/preprints202412.0199.v1

Figure 5. Schematic model showing how the parent **FAU** zeolite transforms to a hierarchal pseudomorphic FAU zeolite or to **MER** zeolite by controlling the temperature of IZT.

Figure 6 shows SEM images of **EDI** zeolite obtained through IZT under different conditions. The **FAU**-**EDI** transformation (KOH/**FAU** = 8.94 and H_2O/KOH = 0.87) at 60 ºC, regardless of the synthesis time (6 or 22 hours), results in nanoparticles **(Figures 6a,b)**. At 80 ºC, short synthesis times (1 hour) also lead to nanoparticles **(Figure 6c)**, but when the synthesis time is increased to 6 hours, larger prismatic particles form **(Figure 6d). Figure 6e,f** shows **EDI** zeolite obtained at 160 ºC (KOH/**FAU** = 2.0 and H_2O/KOH = 2.0), after 5 and 10 min of crystallization, respectively. Despite the relatively short crystallization times, the **EDI** zeolite forms well-shaped, intergrown prismatic particles that range from submicron to micrometric sizes. These results demonstrate that, although the higher temperature accelerates the crystallization process, faster crystallization does not result in smaller crystals.

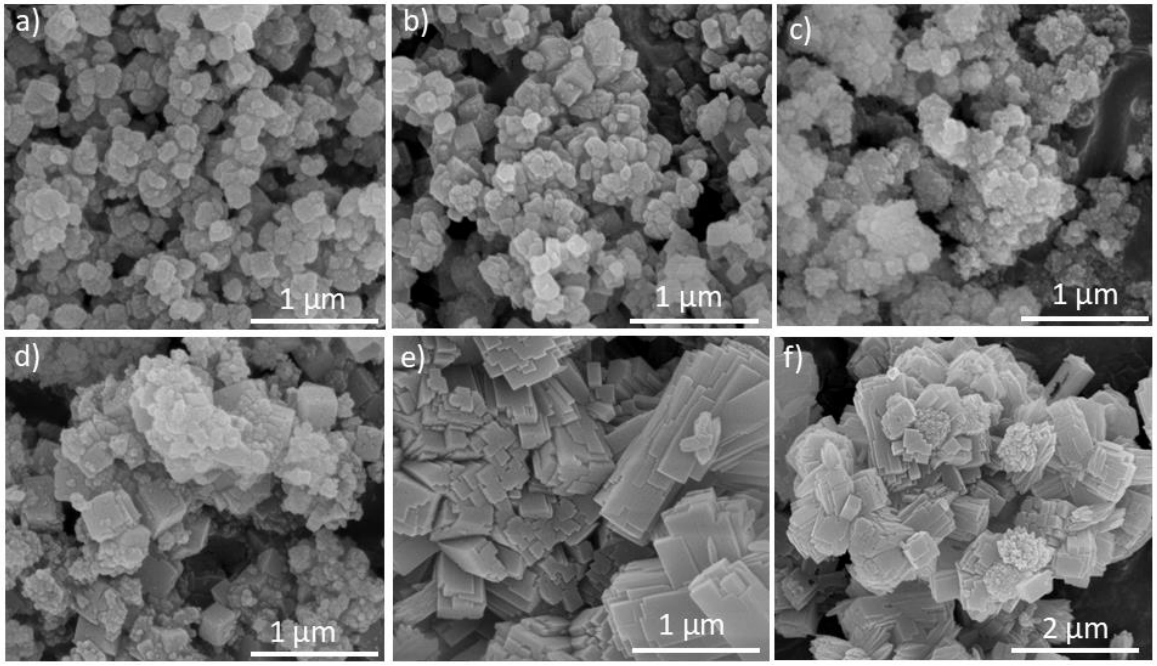

Figure 6. SEM images of **EDI** zeolites obtained by IZT in the system KOH/**FAU** = 8.94 and H_2O/KOH = 0.87 at **(a)** 60 ºC/6h, **(b)** 60 ºC/22h, **(c)** 80 ºC/1h, **(d)** 80 ºC/6h. EDI zeolites obtained in the system KOH/**FAU** = 2 and H_2O/KOH = 2 at **(e)** 160 ºC/5 min and **(f)** 160 ºC/10 min.

Figure 7a,b shows SEM images of ANA zeolites synthesized by the transformation of FAU zeolite under two different conditions: (1) 170 ºC for 1 hour (with CsOH/**FAU** = 2.7 and H_2O/CsOH = 2.59) **(Figure 7a)** and (2) 160 ºC for 10 min (with CsOH/**FAU** = 1.42 and H_2O/CsOH = 4.9) **(Figure 7b)**. In both cases, **ANA** zeolite crystallizes as aggregates of submicron, sphere-like particles. In the first system (170 ºC for 1 hour), the submicron particles are decorated with second-generation nanoparticles (50-70 nm). This feature is absent in the second system (160 ºC for 10 min), suggesting that the differences in supersaturation lead to secondary nucleation and growth in the first system, but not in the second. Additionally, in a system where NaOH/**FAU** = 2 and H_2O/NaOH = 4.5, **FAU** zeolite transforms into a **CAN**-type structure at 160 ºC in 10 min. The resulting phase crystallizes as micrometric intergrowths of prismatic crystals, which is typical for **CAN**-type materials [33].

 doi:10.20944/preprints202412.0199.v1

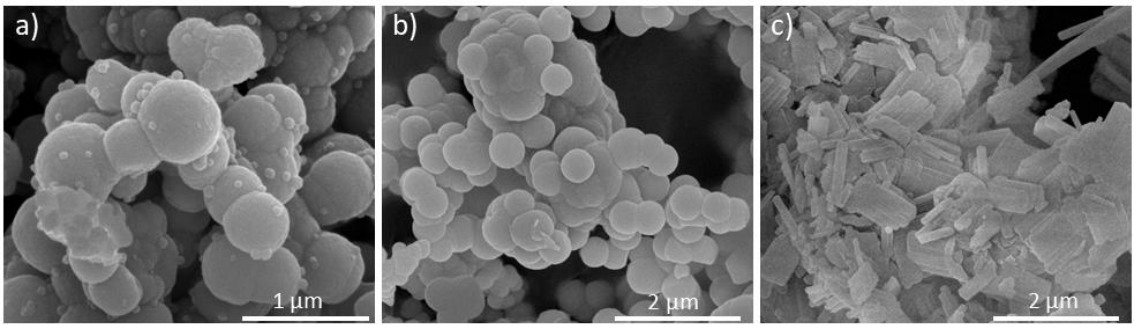

Figure 7. SEM images of **(a) Cs-ANA** zeolite obtained at 170 °C/1h in the system **CsOH/FAU** = 2.7 and H_2O/**FAU** = 2.59, **(b) Cs-ANA** zeolite obtained at 160 °C/10 min in the system CsOH/**FAU** = 1.24 and H_2O/**FAU** = 4.9 and **(c) CAN** zeolite obtained at 160 °C/10 min the system NaOH/**FAU** = 2 and H_2O/**FAU** = 4.5.

3. Experimental

The IZT transformations were performed using a parent FAU zeolite with Si/Al ratio close to 3.0 (±0.1) synthesized by a previously reported procedure [6]. The obtained parent phase was placed in alkaline solutions of NaOH (≥98%, Sigma-Aldrich), KOH (90%, Sigma-Aldrich), and $CsOH{\cdot}H_2O$ (≥90%, Sigma-Aldrich) following the conditions described in **Table 2**. As a base for all synthesis was used 0.5 g of **FAU** zeolite. The crystallization was performed using a microwave reactor Monowave 400 (Anton Paar) and a SiC autoclave. The time for reaching the desired temperature was 5 min for all synthesis. After the synthesis, each sample was filtered and washed with distilled water.

The powder X-ray diffraction (XRD) patterns were obtained using a Bruker D8 Discover diffractometer working with copper radiation (λ_1 = 1.5406 Å, λ_2 = 1.5444 Å) in θ-2θ mode and using step size 0.04°, time per step 0.2 s and a LynxEye detector. Phase identification and quantification were carried out using the EVA software (Bruker AXS) with integrated database of the International Center for Diffraction Data (ICDD). Unit cell parameters were refined using the Le Bail method with TOPAS-3 (Bruker AXS) software. The Si/Al ratios in the **FAU** samples were calculated by the Breck-Flanigen correlation: $Si/Al = ((192 \times 0.00868)/(a_0 - 24.191)) - 1)$ [34]. Scanning electron microscopy (SEM) micrographs and energy dispersive spectroscopy (EDS) chemical analysis were performed on a NanoSEM-FEI Nova 200 equipped with an EDAX Pegasus X4M detector.

4. Conclusions

This work introduces microwave radiation in the synthesis of zeolites by interzeolite transformation. This approach provides control over the particle size and fast access to zeolite structures such as **EDI**, **MER**, **ANA** and **CAN**. An additional derivate of the microwave-assisted IZT is the introduction of an alternative pathway to hierarchical faujasites by fast desilication of a parent zeolite in a short time. In perspective, further development of the microwave-assisted IZT is expected to result in other zeolite framework types.

Supplementary Materials: The following supporting information can be downloaded at the website of this paper posted on Preprints.org.

Funding: This research was funded by Fundação para a Ciência e Tecnologia: UIDB/04650/2020–2023.

Institutional Review Board Statement: Not applicable.

Informed Consent Statement: Not applicable.

Data Availability Statement: The data presented in this study are available in this article.

Acknowledgments: S.F. thanks SEMAT (University of Minho) for the support.

Conflicts of Interest: The author declares no conflicts of interest.

References

1. Mallette, A.J.; Shilpa, K.; Rimer, J.D. The Current Understanding of Mechanistic Pathways in Zeolite Crystallization. *Chemical Reviews* **2024**, *124*, 3416-3493, doi:10.1021/acs.chemrev.3c00801.
2. Ferdov, S.; Shivachev, B.; Koseva, I.; Petrova, P.; Petrova, N.; Titorenkova, R.; Nikolova, R. Metastable microporous lanthanide silicates – Light emitters capable of 3D-2D-3D transformations. *Chemical Engineering Journal* **2024**, *492*, 152355, doi:https://doi.org/10.1016/j.cej.2024.152355.
3. Rocha, J.; Anderson, M.W. Microporous titanosilicates and other novel mixed octahedral-tetrahedral framework oxides. *European Journal of Inorganic Chemistry* **2000**, 801-818.
4. Barrer, R.; Hinds, L.; White, E. 299. The hydrothermal chemistry of silicates. Part III. Reactions of analcite and leucite. *Journal of the Chemical Society (Resumed)* **1953**, 1466-1475.
5. Sano, T.; Itakura, M.; Sadakane, M. High Potential of Interzeolite Conversion Method for Zeolite Synthesis. *Journal of the Japan Petroleum Institute* **2013**, *56*, 183-197, doi:10.1627/jpi.56.183.
6. Ferdov, S. Interzeolite Transformation from FAU-to-EDI Type of Zeolite. *Molecules (Basel, Switzerland)* **2024**, *29*, 1744.
7. Devos, J.; Robijns, S.; Van Goethem, C.; Khalil, I.; Dusselier, M. Interzeolite Conversion and the Role of Aluminum: Toward Generic Principles of Acid Site Genesis and Distributions in ZSM-5 and SSZ-13. *Chem. Mater.* **2021**, *33*, 2516-2531, doi:10.1021/acs.chemmater.0c04832.
8. Jain, R.; Mallette, A.J.; Rimer, J.D. Controlling Nucleation Pathways in Zeolite Crystallization: Seeding Conceptual Methodologies for Advanced Materials Design. *J Am Chem Soc* **2021**, *143*, 21446-21460.
9. Pornsetmetakul, P.; Coumans, F.J.A.G.; Heinrichs, J.M.J.J.; Zhang, H.; Wattanakit, C.; Hensen, E.J.M. Accelerated Synthesis of Nanolayered MWW Zeolite by Interzeolite Transformation. *Chemistry – A European Journal* **2024**, *30*, e202302931, doi:https://doi.org/10.1002/chem.202302931.
10. Mendoza-Castro, M.J.; De Oliveira-Jardim, E.; Ramírez-Marquez, N.-T.; Trujillo, C.-A.; Linares, N.; García-Martínez, J. Hierarchical Catalysts Prepared by Interzeolite Transformation. *J. Am. Chem. Soc.* **2022**, *144*, 5163-5171, doi:10.1021/jacs.2c00665.
11. Barbosa, J.C.; Correia, D.M.; Salado, M.; Gonçalves, R.; Ferdov, S.; de Zea Bermudez, V.; Costa, C.M.; Lanceros-Mendez, S. Three-Component Solid Polymer Electrolytes Based on Li-Ion Exchanged Microporous Silicates and an Ionic Liquid for Solid-State Batteries. *Advanced Engineering Materials n/a*, 2200849, doi:https://doi.org/10.1002/adem.202200849.
12. Bruter, D.V.; Pavlov, V.S.; Ivanova, I.I. Interzeolite Transformations as a Method for Zeolite Catalyst Synthesis. *Petroleum Chemistry* **2021**, *61*, 251-275, doi:10.1134/S0965544121030105.
13. Van Tendeloo, L.; Gobechiya, E.; Breynaert, E.; Martens, J.A.; Kirschhock, C.E.A. Alkaline cations directing the transformation of FAU zeolites into five different framework types. *Chem. Commun.* **2013**, *49*, 11737-11739, doi:10.1039/C3CC47292B.
14. Chengyu, H.W., Yan; Ruren, Xu Crystal transformation behavior of Y-type zeolite under hydrothermal conditions. *Acta Chimica Sinica* **2017**, *75*, 679-685, doi:10.6023/a17040169.
15. Jakupec, N.; Ardila-Fierro, K.J.; Martinez, V.; Halasz, I.; Volavšek, J.; Algara-Siller, G.; Etter, M.; Valtchev, V.; Užarević, K.; Palčić, A. Mechanochemically Induced OSDA-Free Interzeolite Conversion. *ACS Sustainable Chemistry & Engineering* **2024**, *12*, 5220-5228, doi:10.1021/acssuschemeng.3c08477.
16. Pérez González, N.K.; Díaz Guzmán, D.; Vargas Ramírez, M.; Legorreta García, F.; Chávez Urbiola, E.A.; Trujillo Villanueva, L.E.; Ramírez Cardona, M. Interzeolite conversion of a clinoptilolite-rich natural zeolite into merlinoite. *Boletín de la Sociedad Española de Cerámica y Vidrio* **2024**, doi:https://doi.org/10.1016/j.bsecv.2024.04.001.
17. Chiyoda, O.; Davis, M.E. Hydrothermal conversion of Y-zeolite using alkaline-earth cations. *Micropo. Mesopor. Mater.* **1999**, *32*, 257-264, doi:https://doi.org/10.1016/S1387-1811(99)00112-2.
18. Wang, Y.; Li, X.; Xue, Z.; Dai, L.; Xie, S.; Li, Q. Preparation of Zeolite ANA Crystal from Zeolite Y by in Situ Solid Phase Iso-Structure Transformation. *The Journal of Physical Chemistry B* **2010**, *114*, 5747-5754, doi:10.1021/jp907706c.
19. Hu, Z.; Zhao, B.; Zhang, S.; Tan, Z.; Liu, X.; Cao, J. Rapid and high efficient synthesis of zeolite W by gel-like-solid phase method. *Microporous and Mesoporous Materials* **2019**, *281*, 75-83, doi:https://doi.org/10.1016/j.micromeso.2019.03.008.
20. Novembre, D.; Gimeno, D. Synthesis and characterization of analcime (ANA) zeolite using a kaolinitic rock. *Scientific Reports* **2021**, *11*, 13373, doi:10.1038/s41598-021-92862-0.
21. Ferdov, S.; Marques, J.; Tavares, C.J.; Lin, Z.; Mori, S.; Tsunoji, N. UV-light assisted synthesis of high silica faujasite-type zeolite. *Micropo. Mesopor. Mater.* **2022**, *336*, doi:10.1016/j.micromeso.2022.111858.
22. Shi, D.; Xu, L.; Chen, P.; Ma, T.; Lin, C.; Wang, X.; Xu, D.; Sun, J. Hydroxyl free radical route to the stable siliceous Ti-UTL with extra-large pores for oxidative desulfurization. *Chemical Communications* **2019**, *55*, 1390-1393, doi:10.1039/C8CC09225G.
23. Chen, X.; Qiu, M.; Li, S.; Yang, C.; Shi, L.; Zhou, S.; Yu, G.; Ge, L.; Yu, X.; Liu, Z.; et al. Gamma-Ray Irradiation to Accelerate Crystallization of Mesoporous Zeolites. *Angewandte Chemie International Edition* **2020**, *59*, 11325-11329, doi:https://doi.org/10.1002/anie.202002886.

24. Yoshioka, T.; Liu, Z.; Iyoki, K.; Chokkalingam, A.; Yonezawa, Y.; Hotta, Y.; Ohnishi, R.; Matsuo, T.; Yanaba, Y.; Ohara, K.; et al. Ultrafast and continuous-flow synthesis of AFX zeolite via interzeolite conversion of FAU zeolite. *Reaction Chemistry & Engineering* **2021**, *6*, 74-81, doi:10.1039/D0RE00219D.
25. Cheong, Y.-W.; Wong, K.-L.; Ling, T.C.; Ng, E.-P. Rapid synthesis of nanocrystalline zeolite W with hierarchical mesoporosity as an efficient solid basic catalyst for nitroaldol Henry reaction of vanillin with nitroethane. *Materials Express* **2018**, *8*, 463-468, doi:10.1166/mex.2018.1454.
26. Tatlier, M.; Barış Cigizoglu, K.; Tokay, B.; Erdem-Şenatalar, A. Microwave vs. conventional synthesis of analcime from clear solutions. *Journal of Crystal Growth* **2007**, *306*, 146-151, doi:https://doi.org/10.1016/j.jcrysgro.2007.04.056.
27. Sathupunya, M.; Gulari, E.; Wongkasemjit, S. Microwave preparation of Li-zeolite directly from alumatrane and silatrane. *Materials Chemistry and Physics* **2004**, *83*, 89-95, doi:https://doi.org/10.1016/j.matchemphys.2003.09.023.
28. Khomyakov, A.P.; Nechelyustov, G.N.; Sokolova, E.; Bonaccorsi, E.; Merlino, S.; Pasero, M. Megakalsilite, a New Polymorph of KAlSiO4 from the Khibina Alkaline Massif, Kola Peninsula, Russia: Mineral Description and Crystal Structure. **2002**.
29. Yuan, J.; Ma, H.; Luo, Z.; Ma, X.; Guo, Q. Synthesis of KAlSiO4 by Hydrothermal Processing on Biotite Syenite and Dissolution Reaction Kinetics. *Minerals* **2021**, *11*, 36.
30. Verboekend, D.; Nuttens, N.; Locus, R.; Van Aelst, J.; Verolme, P.; Groen, J.C.; Pérez-Ramírez, J.; Sels, B.F. Synthesis, characterisation, and catalytic evaluation of hierarchical faujasite zeolites: milestones, challenges, and future directions. *Chemical Society Reviews* **2016**, *45*, 3331-3352, doi:10.1039/C5CS00520E.
31. Verboekend, D.; Vilé, G.; Pérez-Ramírez, J. Hierarchical Y and USY Zeolites Designed by Post-Synthetic Strategies. *Advanced Functional Materials* **2012**, *22*, 916-928, doi:https://doi.org/10.1002/adfm.201102411.
32. Ferdov, S. Conventional synthesis of layer-like zeolites with faujasite (FAU) structure and their pathway of crystallization. *Micropo. Mesopor. Mater.* **2020**, *303*.
33. Amin, I.I.; Wahab, A.W.; Mukti, R.R.; Taba, P. Synthesis and characterization of zeolite type ANA and CAN framework by hydrothermal method of Mesawa natural plagioclase feldspar. *Applied Nanoscience* **2023**, *13*, 5389-5398, doi:10.1007/s13204-022-02756-4.
34. Breck, D.W.F., E.M. Synthesis and properties of union carbide zeolites L, X and Y. In *Molecular Sieves*; Society of Chemical Industry: London, 1968; pp. 47-60.